Transient Electric Dichroism Studies of Nucleosomal Particles†

D. M. Crothers,* N. Dattagupta, M. Hogan, L. Klevan, and K. S. Lee

ABSTRACT: We report transient electric dichroism experiments on nucleosomal core particles containing 140 and 175 base pairs of DNA, and on spacerless dinucleosomes. The results indicate that all particles possess a permanent dipole moment. The orientation time of 140 base pair nucleosomes implies an estimated maximum dimension of a = 130 Å (a must be at least 111 Å), consistent with the disk model. The maximum dimension of the spacerless dinucleosome is estimated to be about 290 Å (at least 180 Å), ruling out a structure in which two disks are stacked directly on top of each other. The reduced dichroism amplitude indicates that the DNA superhelix axis in nucleosomes aligns perpendicular to the electric field, as expected for a dipole moment directed along a C_2 symmetry axis across the disk diameter. Nucleosomes containing 175 base pairs of DNA show a substantially larger dichroism amplitude than do 140 base pair nucleosomes. In the context of the disk model, this result is shown to be consistent with 100 base pairs of DNA per superhelical turn, but not with 80 base pairs per turn.

The size and shape of nucleosomes, and their arrangement in chromatin, are problems of intense current interest. The model of nucleosomal core particle structure that has emerged from X-ray diffraction (Finch et al., 1977), electron microscopy (Langmore & Wooley, 1975), and neutron scattering studies (Hjelm et al., 1977; Pardon et al., 1975; Suau et al., 1977) is a disk-like object about 110 Å across and 57 Å thick, with histones H2A, H2B, H3, and H4 at the core and DNA wrapped in a superhelix around the circumference. Structural problems still unsolved are the spacial relationship between successive H1-containing nucleosomes in chromatin, and between H1-depleted nucleosomes in the spacerless interaction mode, for which the dimer was isolated and characterized by Klevan & Crothers (1977).

Electric dichroism is a technique of considerable potential utility for addressing such questions because it is highly sensitive not only to the size and shape of a macromolecular species, but also to the angular disposition of the nucleic acid bases relative to the macromolecular orientation axis in the electric field. We describe here electric dichroism measurements on both nucleosomal core particles containing different lengths of DNA, and on spacerless dinucleosomes. In each case analysis of the time required for the particle to orient in the field gives information about the particle's size and shape. The magnitude of the dichroism, when extrapolated to perfect molecular orientation at infinite field, reveals the mean square projection of the UV transition moments of the bases on the axis of orientation in the field. A preliminary account of these results has been communicated (Klevan et al., 1977).

Conversion of dichroism amplitudes to structural parameters such as the superhelix pitch angle requires some extension of existing theory, specifically (a) to treat particles which align with their superhelical axes in a direction other than parallel to the field, and (b) to allow for superhelices that have a nonintegral number of half turns and therefore cannot be considered to possess cylindrical optical symmetry about the superhelix axis. Furthermore, in interpreting dichroism amplitudes, one must recognize the potential for loss of cylindrical optical symmetry of the DNA double helix because of its periodic distortion by bending and by contacts with the histone proteins. In the theoretical section that follows some standard results (Fredericq & Houssier, 1973; Ding et al., 1972; Allen & Van Holde, 1971; Maestre & Kilkson, 1965; Rill, 1972) are rederived briefly in order to provide a coherent basis for our extension of the theory.

Theory

Extinction Coefficients. Recall that the extinction coefficient ϵ of an absorbance transition moment oriented at an angle θ to the direction of the polarization of the electric field vector is proportional to the squared projection of the transition moment on the polarization direction, or

$$\epsilon = \epsilon_0 \cos^2 \theta \tag{1}$$

in which ϵ_0 is the extinction coefficient when the transition moment is parallel to the electric vector. We define the reduced extinction coefficient $\bar{\epsilon}$ as

$$\bar{\epsilon} = \frac{\epsilon}{\epsilon_0} = \cos^2 \theta \tag{2}$$

so that $\bar{\epsilon}$ depends only on geometric factors. Because of the Pythagorean theorem, the sum of the squared projections of the reduced (unity) transition moment on the rectangular coordinate axes must be unity:

$$\bar{\epsilon}_x + \bar{\epsilon}_y + \bar{\epsilon}_z = 1 \tag{3}$$

For a set of identical transition moments oriented randomly, the sum of the average squared projections $\langle \bar{\epsilon}_x \rangle$, etc., also must be unity. Furthermore, because random orientation implies $\langle \bar{\epsilon}_x \rangle = \langle \bar{\epsilon}_y \rangle = \langle \bar{\epsilon}_z \rangle$, the reduced average extinction coefficient $\bar{\epsilon}_r$ for a randomly oriented chromophore is

$$\langle \bar{\epsilon}_x \rangle = \bar{\epsilon}_r = \frac{1}{3} \tag{4}$$

Application of an electric field produces orientation of a molecular axis, taken to be the z axis, along the field direction, but permits free rotation about the z axis. Let $\bar{\epsilon}_z$ be the reduced extinction coefficient for light polarized parallel to the z molecular axis, and $\bar{\epsilon}_x$ and $\bar{\epsilon}_y$ be the corresponding quantities for arbitrarily chosen perpendicular axes (Figure 1). The reduced extinction coefficient ϵ for light polarized parallel to the orientation direction is

$$\bar{\epsilon}_\parallel = \bar{\epsilon}_z$$

† From the Department of Chemistry, Yale University, New Haven, Connecticut 06520. *Received April 21, 1978.* Supported by Grant CA 15583 from the National Cancer Insitute.

0006-2960/78/0417-4525$01.00/0

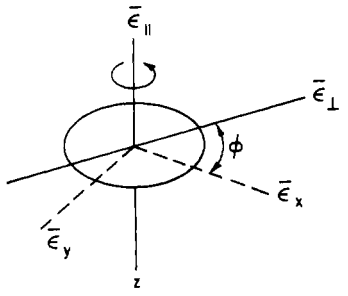

FIGURE 1: Calculation of the reduced extinction coefficient for light polarized parallel and perpendicular to the z molecular axis, assuming free rotation about z. Arbitrarily chosen perpendicular molecular axes x and y rotate freely in the perpendicular plane. The squared projection due to $\bar{\epsilon}_x$ on the perpendicular polarization direction is $\bar{\epsilon}_x \cos^2 \varphi$, and the squared projection due to $\bar{\epsilon}_y$ is $\bar{\epsilon}_y \sin^2 \varphi$. The reduced extinction in the equatorial plane is the sum of these components averaged over all values of θ, or $\bar{\epsilon} = (\bar{\epsilon}_x + \bar{\epsilon}_y)/2$.

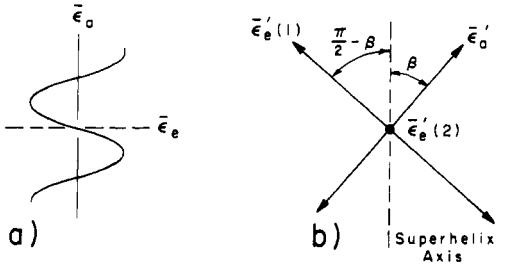

FIGURE 2: Calculation of the axial ($\bar{\epsilon}_a$) and equatorial ($\bar{\epsilon}_e$) reduced extinction components of a superhelix from the axial ($\bar{\epsilon}_a'$) and equatorial ($\bar{\epsilon}_e'$) reduced extinction components of the DNA molecule. (a) View of the superhelix showing $\bar{\epsilon}_a$ directed along the superhelix axis, and $\bar{\epsilon}_e$ in the equatorial plane. (b) Reduced extinction coefficients in an element of the superhelix. $\bar{\epsilon}_a'$ is tangent to the superhelix, and forms an angle β with the superhelix axis. $\bar{\epsilon}_e'(2)$ is perpendicular to the DNA helix and to the superhelix axis (perpendicular to the plane of the drawing). $\bar{\epsilon}_e'(1)$ is also perpendicular to the DNA helix and perpendicular to $\bar{\epsilon}_e'(2)$, lying in the plane of the drawing. The axial reduced extinction component $\bar{\epsilon}_a$ along the superhelix axis is the sum of the components contributed by $\bar{\epsilon}_a'$ and $\bar{\epsilon}_e'(1)$, or $\bar{\epsilon}_a = \bar{\epsilon}_a' \cos^2 \beta + \bar{\epsilon}_e' \cos^2 (\pi/2 - \beta)$. It is assumed that $\bar{\epsilon}_e'(1) = \bar{\epsilon}_e(2) = \bar{\epsilon}_e$ because of rotational averaging of the DNA extinction.

Assuming free rotation about the z axis, the extinction coefficient $\bar{\epsilon}_\perp$ for light polarized perpendicular to the orientation direction is (Figure 1)

$$\bar{\epsilon}_\perp = \frac{1}{2\pi} \int_0^{2\pi} (\bar{\epsilon}_x \cos^2 \varphi + \bar{\epsilon}_y \sin^2 \varphi) d\varphi = \frac{\bar{\epsilon}_x + \bar{\epsilon}_y}{2} \quad (5)$$

Using eq 3, $\bar{\epsilon}_\perp$ can also be expressed as

$$\bar{\epsilon}_\perp = \frac{1 - \bar{\epsilon}_\parallel}{2} \quad (6)$$

The reduced extinction coefficient of a helical array of transition moments, such as provided by the bases in a DNA molecule, can be expressed in terms of the reduced extinction coefficient $\bar{\epsilon}_a'$ directed along the helix axis, and the average reduced extinction $\bar{\epsilon}_e'$ in the equatorial plane, assuming rotational averaging about the helix axis. If α is the angle between a transition moment and the helix axis, eq 1 and 6 yield

$$\bar{\epsilon}_a' = \langle \cos^2 \alpha \rangle \quad (7a)$$

$$\bar{\epsilon}_e' = \frac{1 - \bar{\epsilon}_a'}{2} = \frac{1}{2}(1 - \langle \cos^2 \alpha \rangle) \quad (7b)$$

The extinction components of a DNA molecule coiled into a superhelix are readily calculated (Figure 2). Let $\bar{\epsilon}_a$ and $\bar{\epsilon}_e$ be respectively the reduced extinction coefficients along the superhelix axis and in the perpendicular equatorial plane, the latter averaged for rotation about the superhelix axis. The axial component $\bar{\epsilon}_a$ is made up of contributions from $\bar{\epsilon}_a'$ directed along the DNA axis, and $\bar{\epsilon}_e'$ perpendicular to the DNA axis (Figure 2b), or

$$\bar{\epsilon}_a = \bar{\epsilon}_a' \cos^2 \beta + \bar{\epsilon}_e' \cos^2 \left(\frac{\pi}{2} - \beta\right) \quad (8)$$

in which β is the superhelix pitch angle, $\tan \beta$ = (superhelix circumference/pitch). Insertion of eq 7a and 7b and use of trigonometric identities yield

$$\bar{\epsilon}_a = \frac{1}{2}[1 - \langle \cos^2 \alpha \rangle + \cos^2 \beta (3 \langle \cos^2 \alpha \rangle - 1)] \quad (9a)$$

a result equivalent to that obtained earlier by Rill (1972). The rotationally averaged equatorial extinction coefficient of a superhelix is, by eq 6

$$\bar{\epsilon}_e = \frac{1 - \bar{\epsilon}_a}{2} \quad (9b)$$

A slightly more difficult problem is provided by the case in which the molecule does not have cylindrical optical symmetry; an example is a fractional superhelical turn under orientation conditions that do not allow rotational averaging about the superhelical axis. Figure 3 shows a projection of such an object in a plane perpendicular to the superhelix axis. The axial extinction $\bar{\epsilon}_a$ of an incomplete superhelix is given by eq 9a, but the equatorial extinction coefficient must be calculated separately for the x ($\bar{\epsilon}_{ex}$) and y ($\bar{\epsilon}_{ey}$) molecular axes, rather than computed from $\bar{\epsilon}_a$ as in eq 9b. The reduced extinction coefficient along the x direction contains components due to the squared projection on the x axis of the axial ($\bar{\epsilon}_a'$) and equatorial ($\epsilon_e'(1)$ and $\epsilon_e'(2)$) DNA reduced extinction components. Consideration of Figures 2b and 3 shows that the contribution $d\bar{\epsilon}_{ex}$ to the average extinction given by the DNA contained in $d\theta$ is

$$d\bar{\epsilon}_{ex} = [\bar{\epsilon}_a' \sin^2 \theta \sin^2 \beta d\theta + \bar{\epsilon}_e'(1) \sin^2 \theta \sin^2 \left(\frac{\pi}{2} - \beta\right) d\theta + \bar{\epsilon}_e'(2) \cos^2 \theta d\theta] / \int d\theta \quad (10)$$

Because the DNA is assumed to have cylindrical optical symmetry, $\bar{\epsilon}_e'(1) = \bar{\epsilon}_e'(2)$. Insertion of eq 7b and use of trigonometric identities give

$$d\bar{\epsilon}_{ex} = \frac{\frac{1}{2}[(3\bar{\epsilon}_a' - 1) \sin^2 \theta \sin^2 \beta + 1 - \bar{\epsilon}_a'] d\theta}{\int d\theta} \quad (11)$$

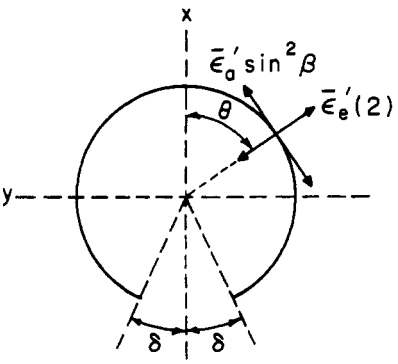

FIGURE 3: Contribution of the axial ($\bar{\epsilon}_a'$) and perpendicular ($\bar{\epsilon}_e'(2)$) reduced extinction along the x direction in an incomplete superhelix. The view is taken along the superhelix axis, normal to the x–y plane. The squared projection due to $\bar{\epsilon}_a'$ on the x–y plane is $\bar{\epsilon}_a' \sin^2 \beta$, so the squared projection on x is $\bar{\epsilon}_a' \sin^2 \beta \sin^2 \theta$. The squared projection due to $\bar{\epsilon}_e'(2)$ on x is $\bar{\epsilon}_e'(2) \cos^2 \theta$. Referring to Figure 2b shows that the squared projection due to $\bar{\epsilon}_e'(1)$ tangent to the superhelix and in the x–y plane is $\bar{\epsilon}_e(1) \sin^2 (\pi/2 - \beta)$. Therefore the squared projection due to $\bar{\epsilon}_e'(1)$ along x is $\bar{\epsilon}_e'(1) \sin^2 (\pi/2 - \beta) \sin^2 \theta$. Addition of these three components yields eq 10.

Integration of eq 11 over $\theta = 0$ to 2π ($\delta = 0$) yields the value of $\bar{\epsilon}_e$ given by eq 9a and 9b, as expected when the number of turns in the superhelix is integral.

When the number of turns in the superhelix is less than 1, $\delta \neq 0$, and θ varies from δ to $2\pi - \theta$. Hence $\bar{\epsilon}_{ex}$ is given by

$$\bar{\epsilon}_{ex} = \frac{1}{4(\pi - \delta)} \int_{\delta}^{2\pi-\delta} [(3\bar{\epsilon}_a' - 1) \sin^2 \beta \sin^2 \theta + 1 - \bar{\epsilon}_a'] d\theta \quad (12)$$

Evaluation of this integral, and substitution of $\langle \cos^2 \alpha \rangle$ for $\bar{\epsilon}_a'$ yields

$$\bar{\epsilon}_{ex} = \frac{(3\langle \cos^2 \alpha \rangle - 1) \sin^2 \beta}{4}(1 + B) + \frac{1 - \langle \cos^2 \alpha \rangle}{2} \quad (13a)$$

in which

$$B = \frac{\sin 2\delta}{2(\pi - \delta)} \quad (13b)$$

Similarly

$$\bar{\epsilon}_{ey} = \frac{(3\langle \cos^2 \alpha \rangle - 1)\sin^2 \beta}{4}(1 - B) + \frac{1 - \langle \cos^2 \alpha \rangle}{2} \quad (13c)$$

Dichroism. The results so far obtained allow us to calculate the dichroism of superhelices oriented parallel or perpendicular to a polarization direction, with rotational freedom about the orientation axis. The equations derived apply to perfect molecular orientation. The reduced linear dichroism ρ is defined (Fredericq & Houssier, 1973) as the ratio

$$\rho = \frac{A_\parallel - A_\perp}{A}$$

in which $A_\parallel$ is the absorbance for light polarized parallel to the orientation direction, and $A_\perp$ is the absorbance for the perpendicular polarization direction. A is the absorbance in absence of orientation. Note that $A_\parallel = \epsilon_\parallel Cl$, $A_\perp = \epsilon_\perp Cl$, and $A = \epsilon_r Cl$, in which C is the concentration and l the path length. By eq 4

$$\epsilon_r = \epsilon_0 \bar{\epsilon}_r = \epsilon_0/3$$

and ρ can be expressed

$$\rho = \frac{3(\epsilon_\parallel - e_\perp)}{\epsilon_0} = 3(\bar{\epsilon}_\parallel - \bar{\epsilon}_\perp) \quad (14a)$$

With eq 6 this equation becomes

$$\rho = \frac{3}{2}(3\bar{\epsilon}_\parallel - 1) \quad (14b)$$

This result can be applied to the possible orientation directions of a superhelix.

Case 1. Orientation parallel to the superhelix axis. In this case

$$\bar{\epsilon}_\parallel = \bar{\epsilon}_a \quad (15a)$$

$$\bar{\epsilon}_\perp = \bar{\epsilon}_e = \frac{1 - \bar{\epsilon}_a}{2} \quad (15b)$$

and the dichroism is, using eq 14

$$\rho_\parallel = \frac{3}{2}(3\bar{\epsilon}_a - 1) \quad (16a)$$

$$= \frac{3}{4}(3 \cos^2 \beta - 1)(3\langle \cos^2 \alpha \rangle - 1) \quad (16b)$$

the latter equation resulting from substitution of eq 9a for $\bar{\epsilon}_a$. Except for a factor 3 that distinguishes dichroism from birefringence, 16b is a subcase of the more general result obtained by Maestre & Kilkson (1965), and is the same as the equation derived by Rill (1972). Two simple limiting cases of eq 16b are (a) a linear DNA molecule oriented parallel to the field, with $\alpha = 90°$, $\beta = 0$, for which $\rho_\parallel = -3/2$, and (b) a DNA circle ($\alpha = 90°$, $\beta = 90°$) oriented in a plane perpendicular to the field, for which $\rho_\parallel = 3/4$.

Case 2. Superhelix axis perpendicular to the direction of orientation. In this case

$$\bar{\epsilon}_\parallel = \bar{\epsilon}_e \quad (17a)$$

$$\epsilon_\perp = \frac{\bar{\epsilon}_a + \bar{\epsilon}_e}{2} \quad (17b)$$

Use of eq 9b and 14 yields for the (perpendicular) dichroism

$$\rho_\perp = \frac{3}{4}(1 - 3\bar{\epsilon}_a) \quad (18a)$$

$$= -\frac{3}{8}(3 \cos^2 \beta - 1)(3\langle \cos^2 \alpha \rangle - 1) \quad (18b)$$

$$= -\frac{1}{2}\rho_\parallel \quad (18c)$$

Two limiting cases of this equation are (a) a linear DNA, with $\alpha = 90°$ and $\beta = 0°$, aligned perpendicular to the field, for which $\rho_\perp = 3/4$, and (b) a DNA circle ($\alpha = 90°$, $\beta = 90°$) whose diameter parallels the field, for which $\rho_\parallel = -3/8$.

Case 3. Incomplete superhelix with axis parallel to orientation direction. In this case, rotation is allowed about the superhelix axis, thus conferring cylindrical optical symmetry on the molecule, and the dichroism is that predicted for case 1.

Case 4. Fractional superhelix with superhelical axis perpendicular to the orientation direction. In this case we assume orientation along the C_2 symmetry axis, the x axis in Figure 3. Therefore

$$\epsilon_\parallel = \bar{\epsilon}_{ex} \quad (19a)$$

$$\epsilon_\perp = \frac{\bar{\epsilon}_{ey} + \bar{\epsilon}_a}{2} \quad (19b)$$

Using eq 9a for $\bar{\epsilon}_a$, and eq 13a and 13c for $\bar{\epsilon}_{ex}$ and $\bar{\epsilon}_{ey}$, substituting into eq 14 and rearranging yield

$$\rho_\perp = -\frac{3}{8}(3\langle \cos^2 \alpha \rangle - 1)(3 \cos^2 \beta - 1 - 3B \sin^2 \beta) \quad (20)$$

in which B is given by eq 13b. When there is more than one superhelical turn, the dichroism is a weighted average of the dichroism of the full turns and the fractional turns, or

$$\rho_\perp = -\frac{3}{8}\frac{(3\langle \cos^2 \alpha \rangle - 1)}{(N + \delta/\pi)}\left\{(N + \delta/\pi)(3 \cos^2 \beta - 1) - \frac{3B\delta \sin^2 \beta}{\pi}\right\} \quad (21)$$

in which N is the number of complete turns.

Higher Order Superhelices. Possible arrangements of DNA in chromatin include superhelical wrapping of the nucleosome-bound DNA fiber, producing another order of superhelical organization. Equations 16 and 18 allow one to calculate the dichroism of a superhelix from the dichroism of the lower order helix (assumed to have cylindrical optical symmetry) and the superhelical pitch angle. Repetition of the derivation for the next order of superhelical organization produces the following recursion relation for the dichroism

when alignment is parallel ($\rho_\parallel$) or perpendicular ($\rho_\perp$) to the superhelix axis:

$$\rho_{\parallel,n} = -\frac{1}{2}\rho_{\parallel,n-1}(3\cos^2\beta_n - 1) \quad (22a)$$

$$\rho_{\parallel,0} = -\frac{3}{2}(3\langle\cos^2\alpha\rangle - 1) \quad (22b)$$

$$\rho_{\perp,n} = -\frac{1}{2}\rho_{\parallel,n} \quad (22c)$$

in which β_n is the pitch angle of the nth order superhelix. Equations 22a and 22b are the equivalent for dichroism of the general relationship obtained for birefringence by Maestre & Kilkson (1965). Note that it is assumed for eq 22a and 22c that the superhelix of order $n-1$ has cylindrical optical symmetry when it is wound into a superhelix of order n.

Asymmetric Orientation of Incomplete Superhelices. Nucleosomes are expected to coil into a superhelix, but, when the number of monomers in a multinucleosome is small, the orientation axis need not be either parallel or perpendicular to the superhelix axis. Furthermore, because the superhelical winding of DNA about the histone core may contain a nonintegral number of turns, one cannot assume cylindrical optical symmetry of the multinucleosome fiber which is coiled into a higher order superhelix. We provide here a formula for calculating the dichroism of an incomplete superhelix oriented at an arbitrary direction relative to the field. From this expression the expected dichroism of any model for a collection of connected nucleosomes can be calculated as a weight-average of the individual contributions.

Let γ_1 be the angle between the field and z axis (the superhelical axis) of an oriented incomplete first-order superhelix. For example, for a disk-shaped nucleosome γ_1 is the angle between the field and the normal to the plane of the disk (the x–y plane). Let the angle γ_2 measure rotation in the x–y plane about the z axis. We set $\gamma_2 = 0$ when the suerphelix is rotated so that the C_2 axis (the x axis in Figure 3) has its maximum projection along the field direction. The reduced extinction for light polarized along the field is a sum of the squared projections on the field direction of the axial and equatorial reduced extinction coefficients of the incomplete superhelix:

$$\epsilon_\parallel = \cos^2\gamma_1\bar{\epsilon}_a + \cos^2\gamma_2\sin^2\gamma_1\,\bar{\epsilon}_{ex} + \sin^2\gamma_2\sin^2\gamma_1\bar{\epsilon}_{ey}$$

Use of eq 9a, 13a–c, and 14b leads to

$$\rho = -\frac{3}{8}(3\langle\cos^2\alpha\rangle - 1)\{(3\cos^2\beta - 1)(1 - 3\cos^2\gamma_1) - 3B\sin^2\beta\sin^2\gamma_1(2\cos^2\gamma_2 - 1)\} \quad (23)$$

Equation 23 applies when the number of turns per incomplete superhelix is one or less; when there is more than one turn, this expression should be averaged with the equivalent expression having $B = 0$, as done to obtain eq 21 from eq 20. Notice that eq 23 reduces to eq 20 when $\gamma_1 = 90°$, $\gamma_2 = 0$, and to eq 16b when $\gamma_1 = 0$.

Equation 23 describes the dichroism of an incomplete first-order superhelix, such as a nucleosomal disk, arbitrarily oriented (as described by γ_1 and γ_2) relative to the field. A long multinucleosomal fiber can be expected to orient with a symmetry axis of the second order superhelix (usually the long axis) parallel to the field. In this case, all the identical elements of the second-order superhelix are equivalent. For example, all disks are equivalent, as are all spacer regions. Equation 23 serves as the basis for calculation of the dichroism contributed by a disk and by a spacer region, assuming a specific model for their orientations relative to the symmetry axis. The total dichroism is a weighted average of the contributions due to the individual elements of the second order superhelix.

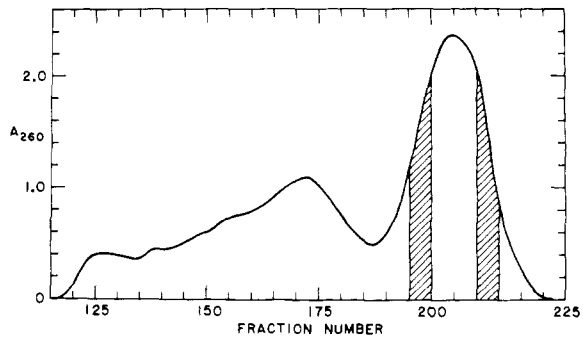

FIGURE 4: Elution profile of a partial nuclease digest of calf thymus nuclei chromatographed on a Bio-Gel A-5M column. The shaded sections show the portions of the mononucleosome peak which were pooled to obtain 175 base pair (early eluting) and 140 base pair (late eluting) nucleosomes.

When there are only a few nucleosomes in the second-order superhelix, the orientation axis may not coincide with a symmetry axis of the second order superhelix. In this case the disk and spacer elements do not form equivalently oriented sets, and separate contributions for each individual disk and spacer must be calculated and added to form a weighted average. This requires a specific model for the orientation direction of the particle, as well as for its structure.

Materials and Methods

Preparation of Nucleosomal Particles. The 140-base pair nucleosomal core particles and spacerless dinucleosomes were prepared by micrococcal nuclease digestion of H1-depleted chromatin as described by Klevan & Crothers (1977). In addition, nucleosomal core particles of two sizes were prepared by micrococcal nuclease digestion of nuclei. Calf thymus nuclei were prepared by modification of the method of Blobel & Potter (1966). A 50-g sample of frozen thymus was minced and homogenized in 200 mL of solution A (0.3 M sucrose, 50 mM triethanolamine, 25 mM KCl, 5 mM $MgCl_2$, and 1 mM $PhCH_2SO_2F$, pH 6.5 at 4 °C) using a Waring blender at 40 V for 5 min. After filtration through cheesecloth, nuclei were pelleted at 800g for 10 min and washed several times with solution A and then with solution B (0.3 M sucrose, 50 mM triethanolamine, 25 mM KCl, 4 mM $MgCl_2$, 1 mM $CaCl_2$, and 1 mM $PhCH_2SO_2F$, pH 7.0 at 37 °C). Nuclei were resuspended in solution B to a concentration of 100 OD_{260} and digested with 400 units of micrococcal nuclease mL^{-1} at 37 °C for 6 min. The digestion was stopped by the addition of EDTA to a final concentration of 5 mM. Nuclei were pelleted by centrifugation at 800g for 10 min and used with lysis buffer (0.2 mM EDTA, 1 mM $PhCH_2SO_2F$, pH 7.5 at 4 °C) using a Pasteur pipet. After centrifugation at 10 000g for 10 min to remove the nuclear debris, the chromatin supernatant was loaded on a Bio-Gel A-5m column. Figure 4 shows an elution profile of the digestion products on the column. The major peak consists of mononucleosomal particles; the shaded fractions were pooled separately to yield samples containing 175 and 140 base pairs of DNA, respectively. Of critical importance for dichroism measurements is the absence of free DNA because of its large negative dichroism. Figure 5 shows 5% polyacrylamide gel electrophoresis of the two mononucleosome fractions and their DNA components, indicating that the particle samples are free of contaminating DNA. Gel electrophoresis of both mononucleosome fractions revealed only trace amounts of histone H1.

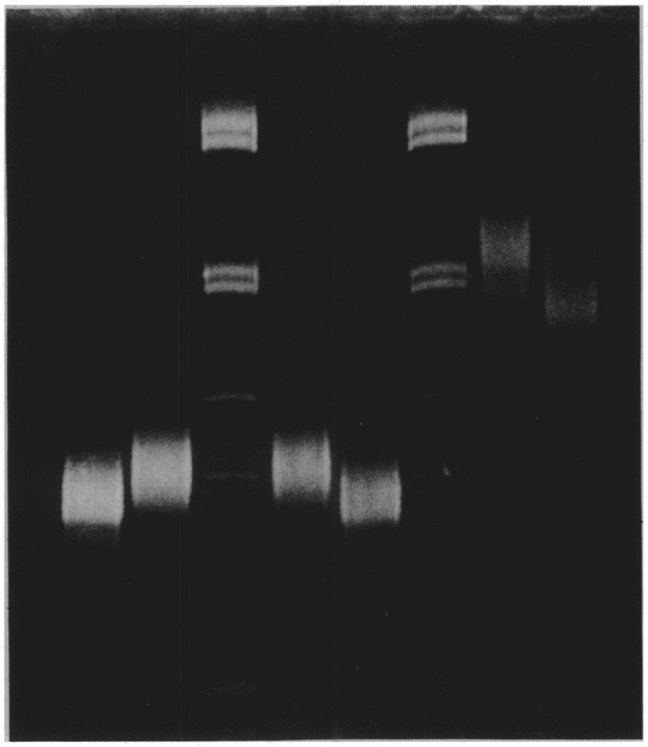

FIGURE 5: Five percent polyacrylamide gel electrophoresis of nucleosomes and DNA. From left to right, 140 BP DNA, 175 BP DNA, *Hae*III restriction digest of Col E1 DNA used as size marker, 175 BP DNA, 140 BP DNA, restriction digest, 175 BP nucleosome, 140 BP nucleosome.

Dichroism Measurements. Dichroism amplitudes and relaxation times were measured on a modified T-jump apparatus as described previously (Hogan et al., 1978). Samples were used immediately after elution from the Bio-Gel A-5m column. The column buffer concentration (10 mM Tris–5 mM EDTA, pH 7.6) was adjusted by dilution with distilled water and addition of stock solutions of added materials such as dextran (Pharmacia, T 500). Except where specifically noted, dichroism measurements were made on samples of concentration 2–5 × 10^{-5} M in base pairs, dissolved in 2.5 mM Tris-HCl, 1.25 mM Na_2EDTA, pH 7.6 at 7 °C. Under these conditions no measurable changes in dichroism amplitude or relaxation time could be detected when the sample concentration was varied or when the sample was exposed to repeated applications of high electric fields (up to 35 kV cm^{-1}).

Analysis of Orientation Times. Dichroism does not appear instantaneously when the field is turned on, since macromolecular rotation is required for orientation. Tinoco (1955) showed that the rise of the dichroism should follow the general equation

$$\frac{\rho(t)}{\rho(\mathrm{ss})} = 1 - \frac{3B' \exp(-2D_r t)}{(2B'+1)} + \frac{(B'-2)\exp(-6D_r t)}{2(B'+1)} \qquad (24)$$

in which $\rho(t)$ is the reduced dichroism at time t, $\rho(\mathrm{ss})$ is the limiting steady-state value at a given field, B' is the ratio of permanent to induced moment contributions to the orientation, and D_r is the rotational diffusion constant. In the case of DNA there is no permanent dipole moment, and $B' = 0$, so $\rho(t)$ should rise with $\exp(-6D_r t)$, as confirmed by Hogan et al. (1978). Hence

$$\tau = (6D_r)^{-1} \text{ (no permanent moment)} \qquad (25a)$$

When a permanent dipole moment is present in the molecule, the long time portion of the rise curve depends on $\exp(-2D_r t)$, so the observed time τ is related to D_r by

$$\tau = (2D_r)^{-1} \text{ (permanent dipole)} \qquad (25b)$$

Field Dependence of the Dichroism. The dependence of the steady-state dichroism on the electric field is determined by the orientation mechanism. O'Konski et al. (1959) expressed the ratio of the dichroism at field E, ρ_E, to that at infinite field, ρ_∞, by the orientation function $\Phi = \rho_E/\rho_\infty$. When orientation is dominated by a permanent dipole moment, Φ is given by (O'Konski et al., 1959)

$$\Phi = 1 - \frac{3kT}{\mu E}\left[\coth(\mu E/kT) - kT/\mu E\right] \qquad (26a)$$

in which μ is the dipole moment. When orientation is dominated by an induced moment, Φ is given by (O'Konski et al., 1959)

$$\Phi = \frac{3}{4}\left(\frac{\exp\gamma}{\gamma F(\sqrt{\gamma})} - \frac{1}{\gamma}\right) - \frac{1}{2} \qquad (26b)$$

in which $F(\sqrt{\gamma})$ is an integral and $\gamma = (\alpha_1 - \alpha_2)E^2/(2kT)$, α_1 and α_2 being respectively the polarizabilities parallel and perpendicular to the molecular symmetry axis. Hogan et al. (1978) recently suggested a third orientation mechanism in which the torque arises from loss of cylindrical symmetry of the ion atmosphere because of anisotropic ion flow. In this case the orientation function is described by eq 26b, but γ is redefined as $\gamma = AE/kT$ with A a constant having the dimensions of a dipole moment. The anisotropic ion flow model fits the field-dependence data for DNA with A proportional to the square of DNA length and also proportional to the Debye radius in the solution (Hogan et al., 1978).

Results

The Field Dependence of the Dichroism Is Consistent with a Permanent Dipole Orientation Mechanism. Figures 6a and 6b show the dichroism amplitude of 140 BP nucleosomes and spacerless dinucleosomes as functions of the electric field. Comparison is made with theoretical curves adjusted for best fit to the permanent moment, induced monent, and ion flow models. The ion flow model clearly can be excluded by its failure to predict correctly the field dependence. Of the remaining two models, orientation by a permanent moment fits the data at all values of the field, whereas the induced moment model shows marginal deviations from the data at low field.

The Apparent Dipole Moment Does Not Vary with Increased Salt Concentration. Increasing the ionic strength of the dichroism buffer from 2 to 5 mM had no effect on the measured dichroism at each value of the field, and therefore no effect on the apparent dipole moment. For comparison the apparent dipole moment of DNA decreases by about a factor of two over the same salt concentration range (Hogan et al., 1978). Generally, induced dipole moment orientation is found to depend on salt concentration (Minakata et al., 1972), so the failure to find a salt concentration effect for nucleosomes favors the permanent dipole mode. As shown below, only the permanent moment model produces good agreement between the dimensions of nucleosomes calculated from the orientation time and measured by other techniques.

Nucleosomal Particles Differ in Their Extrapolated Dichroism. Figures 6a and 6b show that the limiting dichroism of a 140 BP nucleosome is −0.29, whereas the spacerless dimer has a limiting value of −0.12, determined in both cases by extrapolation using the orientation equation for a permanent dipole moment. Figure 7 shows a comparison of dichroism amplitudes for 140 BP and 175 BP nucleosomes, using in this case a plot against the reciprocal electric field. Extrapolation

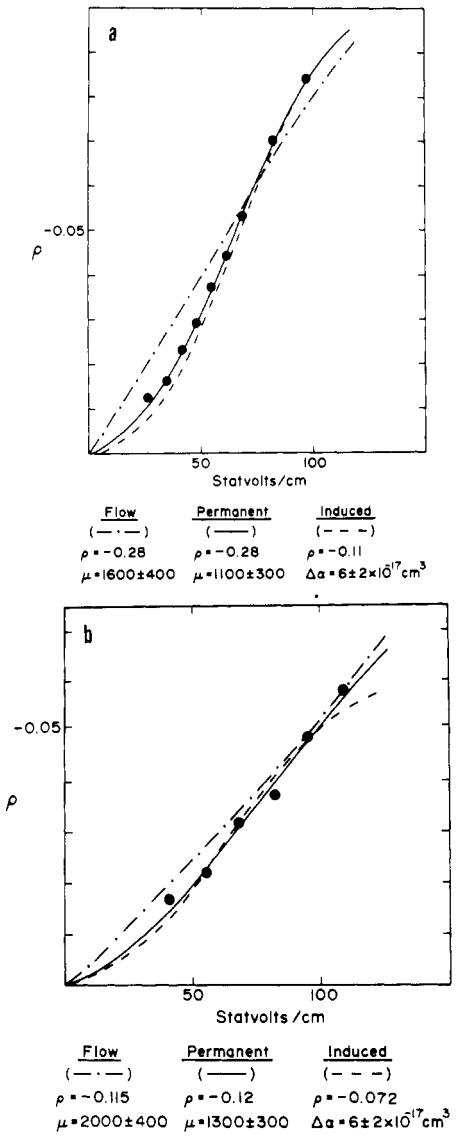

FIGURE 6: Comparison of dichroism amplitudes with three models for the orientation mechanism, whose parameters were adjusted for best fit. (– · –) Ion flow model; (—) permanent moment model; (- - -) induced moment model; T = 7 °C. (a) The 140 BP nucleosome. Parameters: ion flow model, $\rho_\infty = -0.28$, μ = 1600 D; permanent moment model, $\rho_\infty = -0.28$, μ = 1100 D, induced moment model, $\rho_\infty = -0.11$, $\Delta\alpha = 6 \times 10^{17}$ cm^3. (b) The 250 BP spacerless dinucleosome. Parameters: ion flow model, $\rho_\infty = -0.115$, μ = 2000 D; permanent moment model, $\rho_\infty = -0.12$, μ = 1300 D; induced moment model, $\rho_\infty = -0.072$, $\Delta\alpha = 6 \times 10^{-17}$ cm^3.

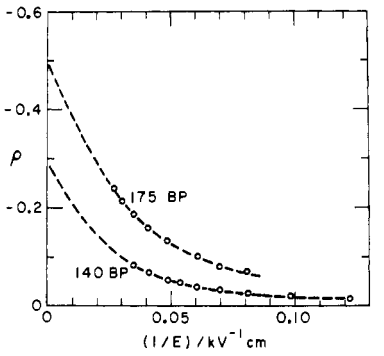

FIGURE 7: Field dependence of the dichroism amplitudes of 140 and 175 BP nucleosomes. The dashed lines are the theoretical curves for the permanent dipole moment orientation mechanism.

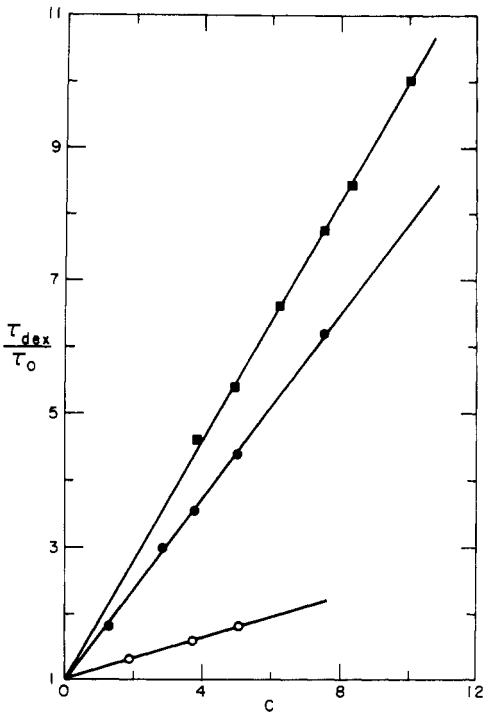

FIGURE 8: Dextran dependence of the orientation time of nucleosomes and DNA. τ_{dex}/τ_0 is the ratio of the time τ_{dex} observed in dextran solution to the extrapolated value τ_0. For both DNA (○) and spacerless dinucleosome (●), the extrapolated value agrees with the value measured without dextran, but the value measured for 140 BP nucleosome (■) in absence of dextran is appreciably larger than the extrapolated value. C is the dextran concentration in g/mL.

using the permanent dipole moment equation yields a value of −0.49 for the 175 BP nucleosome. Evidently the additional 35 BP of DNA added to the 140 BP nucleosome has a strong tendency to align with the double helix axis parallel to the electric field, thus contributing a strong incremental negative dichroism in the 175 BP particle. An important control on this measurement is the absence of free DNA in the gel electrophoresis pattern of the nucleosomal particles shown in Figure 5, since free DNA would strongly alter the observed dichroism.

Rotational Correlation Times Can Be Determined by Extrapolation of Data Measured in Dextran Solutions. The smallest rotational diffusion constant of a macromolecule depends on roughly the third power of its major dimension, allowing accurate determination of macromolecular size by measurement of the rotational orientation time. However, it is essential that one demonstrate that the transient dichroism rise time is indeed limited by frictional resistance to rotation. For this purpose we added a neutral polymer, dextran, in order to obtain substantial viscosity enhancement with minimum alteration of solvent properties. Generally, we found a linear relationship between the observed exponential time constant τ of the dichroism rise and the weight concentration of dextran in the sample. Since the relationship of τ to bulk viscosity η was *not* linear, rotational motion must be responding to an effective microscopic viscosity that is linear in dextran concentration. An interesting feature of the results is shown in Figure 8, in which the ratio of τ measured in dextran to the extrapolated value at zero concentration is plotted against dextran concentration. Nucleosomes, which are much more spherical in shape than the highly elongated DNA double helix, are much more strongly inhibited from rotation by added dextran than is DNA. The inference that the effective microscopic viscosity depends on particle shape is strengthened by the observation (Klevan et al., 1978) that the highly extended (H3-H4)$_2$–DNA

TABLE I: Dichroism and Rotational Relaxation Properties of Nucleosomal Particles.

sample	ρ_∞ [a]	μ_{ap} [b] (D)	τ [c] (μs)	$\tau_{20,w}$ [d] (μs)	a_{min} [e] (Å)	τ/τ_0 [f]	a/b [g]	a (Å) [h]
DNA 140 BP	−1.1	4900 ± 200	3.4 ± 0.2	2.4	260	37	4	480
nucleosome 140 BP	−0.29	1100 ± 200	0.8 ± 0.2	0.6	111	1.4	2.3	130
nucleosome 175 BP	−0.49	1400 ± 300	1.1 ± 0.2	0.8	124			
spacerless dimer, 250 BP	−0.12	1600 ± 300	3.4 ± 0.2	2.4	180	2.9	3.6	290

[a] Limiting reduced dichroism extrapolated to infinite field. [b] Apparent dipole moment for the ion flow model (DNA) or permanent moment orientation mechanism (nucleosomes). [c] Measured time constant for dichroism rise, extrapolated to zero dextran concentration, at 7 °C. [d] τ corrected to water at 20 °C by multiplying by the ratio of viscosities $\eta_{20°C}/\eta_{7°C}$. [e] Minimum value of the length of the long axis of the particle, calculated as the diameter of a sphere having $\tau = \pi\eta a_{min}^3/(2kT)$ for permanent moment orientation and $\tau = \pi\eta a_{min}^3/(6kT)$ for induced dipole orientation (DNA). [f] τ_0 is the value of τ expected for a sphere having the volume of the particle. For DNA, the volume was calculated for a cylinder 476 Å length × 26 Å diameter. The volume of a 140 BP nucleosome was calculated for a cylinder 110 Å diameter × 55 Å height (Finch et al., 1977), and the volume of the spacerless dimer was taken as twice this value. No value was assumed for the 175 BP nucleosome. [g] Axial ratio of the particle, calculated from τ/τ_0 using the equation given by Koenig (1975). It was assumed that τ is the time constant for orientation of the long axis (a) of the particle, that the mononucleosome is an oblate ellipsoid, and the spacerless dimer is a prolate ellipsoid. [h] Length of the long axis of the particle, calculated for DNA from τ using Broersma's (1960) equation for a cylinder, and assuming $a/b = 18.5$. (The calculated value of a is quite insensitive to the assumed value of a/b.) For nucleosomes, a was calculated from a/b (g) and the assumed volume (f). As in g, the 140 BP nucleosome was assumed to be an oblate ellipsoid, and the spacerless dimer was assumed to be a prolate ellipsoid.

complex responds to dextran in a manner similar to the response of DNA, rather than like nucleosomes.

The Rotational Orientation Time of DNA and the Spacerless Dimer Measured in Aqueous Buffer Equals the Extrapolated Values. We found that measurement of τ in absence of dextran gave values of 3.4 μs for 140 BP DNA and 3.4 μs for the spacerless dimer, both in dichroism buffer at 7 °C. These results agree within experimental error (±0.2 μs) with the result obtained by extrapolation of the data in dextran solutions, confirming that the transient dichroism rise in dextran-free buffer is limited by frictional resistance to macromolecular rotation.

The Dichroism Rise Time of Mononucleosomes Measured in Aqueous Buffer Is Slower than the Extrapolated Value. Experiments on nucleosomes in aqueous buffer revealed a rise time for the dichroism of about 2 μs, clearly slower than the value (0.8 ± 0.2 μs, 7 °C) extrapolated from the dextran dependence. We conclude that transient phenomena other than molecular rotation limit the dichroism rise of nucleosomes in aqueous dichroism buffer. All later calculations of the rotational frictional coefficient are based on extrapolation of the dextran-dependent data in the linear range shown in Figure 8.

We have observed a similar disagreement between the results of direct measurement of τ and the dextran extrapolation when measurements are made on DNA samples dissolved in salt concentrations below 1 mM (unpublished work). The nature of these transient phenomena and their relationship to the apparent permanent dipole moment of nucleosomal particles will require further study for elucidation.

Discussion

The Rotational Time Constant of 140 BP Nucleosomes Is in Good Agreement with the Disk Model. We analyzed the rotational relaxation time data for nucleosomal particles in two different ways, as summarized in Table I. (a) With no assumptions about the size of the particle, we calculated the diameter a_{min} of a sphere having the observed rotational relaxation time, $a_{min} = [2kT\tau/\pi\eta]^{1/3}$ for permanent dipole orientation, and $a_{min} = [6kT\tau/\pi\eta]^{1/3}$ for induced dipole orientation. The former equation was used for nucleosomal particles and the latter for DNA. An asymmetric particle whose maximum dimension is a_{min} has a smaller value of τ than a sphere of diameter a_{min}. Hence an asymmetric particle must have its largest dimension $a > a_{min}$ in order to rotate at the observed rate. Thus a_{min} is the smallest possible value of the maximum distance across the particle. No assumptions about particle shape or volume are required for this conclusion. (b) Assuming that nucleosomes have the volume of a disk 110-Å diameter and 55-Å height (Finch et al., 1977), and that the spacerless dimer has a volume twice as large, we calculated the length a of the longest axis of the ellipsoid of revolution that has both the same volume as the particle, and the observed value of τ. An oblate ellipsoid was used as a model for the nucleosomal disk; because the results showed the spacerless dimer to have a greater axial ratio, we chose in that case the model for a prolate ellipsoid. Calculations used the equations given by Koenig (1975).

The results for the 140 BP nucleosome (Table I) show a minimum value of a_{min} = 111 Å for the longest distance across the particle. The oblate ellipsoid that fits the data has as its longest axis a = 130 Å. For comparison, the longest distance across a disk 110-Å wide and 55-Å high is 123 Å, passing from edge to edge through the center of the particle. The axial ratio obtained from our results, 2.3, also is in good agreement with the disk model, based on its ratio of diameter to height = 2.

The Spacerless Dimer Is a Considerably Larger Particle. Results of the same calculation performed for mononucleosomes are also reported for the spacerless dimer in Table I. The minimum diameter a_{min} is 180 Å, and the largest axis of an equivalent prolate ellipsoid is a = 290 Å. These results do not allow us to specify a precise model. However, they clearly rule out a structure in which one mononucleosomal disk is stacked directly on top of another, because the maximum dimension of such a structure is 156 Å.

The Dichroism of 140 BP Nucleosomes Implies Orientation of the Disk Diameter Parallel to the Field. As demonstrated in the theoretical section, orientation of a flattened superhelix of DNA with the superhelix axis (the cylindrical axis of the disk) parallel to the field should produce a dichroism of roughly +¾, whereas orientation with the superhelix axis perpendicular to the field yields ρ of about −⅜. The latter is close to the value measured for 140 BP nucleosomes. Furthermore, any C_2 axis that the nucleosomal disk may possess must be perpendicular to the superhelix axis. A molecule containing a C_2 axis can have a dipole moment only along the C_2 axis, and one therefore predicts orientation of the disk edge-on to the field, with the cylindrical axis perpendicular to the field. Hence the observed

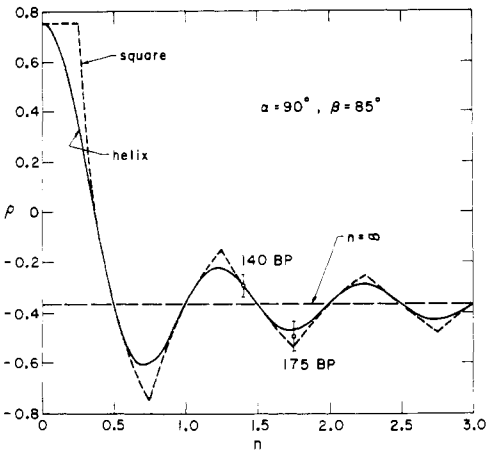

FIGURE 9: Theoretical variation of nucleosome dichroism with number of DNA turns (n) compared with two experimental points. The solid line shows the expected variation (eq 21) if DNA is wound in a superhelical path about a cylindrical disk, and the dashed line shows the effect if the DNA follows a square path. To fit the data, 100 BP were set equal to one turn, with $\alpha = 90°$ and $\beta = 85°$.

reduced dichroism of −0.29 is entirely consistent with the DNA winding and symmetry properties embodied in the disk model.

The Larger Negative Dichroism of 175 BP Nucleosomes Can Be Used to Estimate the Number of Base Pairs per Turn of DNA about the Disk. As shown in Figure 3, the orientation and hence the dichroism of a section of DNA added to an incomplete superhelix oriented along its C_2 axis depend on how many turns the helix contains. For example, if a small piece of DNA is added to a superhelix containing one turn, the added material is oriented perpendicular to the field and causes the dichroism to become more positive. On the other hand, if the superhelix contains 1.5 turns, the added segment is parallel to the field, and the dichroism amplitude should become more negative. Figure 9 shows a calculation of the expected dichroism of nucleosomal disks containing 0–3 turns of DNA, based on eq 21. The superhelix pitch angle β was taken as 85° from the disk model; the calculation is very insensitive to β in this region because $\cos^2 \beta$ is nearly zero. The angle α was chosen at 90° in order to fit the dichroism values of 140 and 175 BP nucleosomes simultaneously.

The substantially greater dichroism amplitude of 175 BP nucleosomes compared with 140 BP particles implies that the 35 added base pairs orient nearly parallel to the C_2 axis. A satisfactory fit to the data is obtained if it is assumed that there are 100 BP per turn of the superhelix. If we restrict our consideration to smooth winding of DNA in a cylindrical path, our results are clearly not consistent with 80 BP per turn as proposed by Finch et al. (1977), because 140 BP would be 1.75 turns and should have a larger dichroism amplitude than 175 BP at 2.2 turns (Figure 9).

It is conceivable that the extra DNA in 175 BP nucleosomes diverges from the cylindrical path, pointing instead along the C_2 axis and causing the dichroism amplitude to increase. Using the criteria of drug binding and drug dichroism (for triphenylmethane dyes, netropsin, distamycin, and ethidium), we were unable to find evidence in 175 BP nucleosomes for DNA sections that have the properties and hence conformation of normal B-form DNA (unpublished results). Hence the extra DNA must be interacting with the histone proteins and cannot be simply protruding into the solution.

An argument in favor of 80 BP per superhelical turn is the 3.4-Å DNA spacing per base pair one calculates at the average radius of about 43 Å. With 100 BP per turn, the spacing is 3.4 Å at nearly the maximum radius of 55 Å. However, it may be energetically advantageous to maintain the 3.4-Å spacing at the outer radius to avoid loss of stacking interactions there. Compression of the base pair spacing to smaller values on the inner radius could be achieved by tilting the bases relative to the local DNA axis.

The angle $\alpha = 90°$ used for the calculation shown in Figure 9 would appear to indicate that the bases are not tilted relative to the local DNA axis. However, we do not believe that this result, which depends on the assumption of cylindrical optical symmetry for the nucleosome-bound DNA, should be taken at face value. More generally stated, the observations imply that the DNA base planes are oriented nearly parallel to the cylindrical axis of the nucleosomal disk. This geometry can be consistent with tilting of the base pairs relative to the DNA axis if there is periodic distortion of the double helix as it turns about its local axis. This might require, for example, that the base tilt be different when the small or large DNA grooves face the outer direction on the nucleosome. Such distortion appears in the structure calculated by Levitt (1978) for DNA bent smoothly about the nucleosomal core proteins. Visual inspection of Levitt's model reveals that the DNA bases are nearly parallel to the superhelical axis, as implied by our results.

Models for the Spacerless Dinucleosome. Our results reveal an asymmetric structure and relatively small negative dichroism amplitude for the spacerless dinucleosome. We earlier suggested the slipped-disk model for the spacerless dimer (Klevan et al., 1977) based on these properties. In this model the disks are stacked on top of each other, but one disk is displaced relative to the other in order to provide a long dimension of adequate length. The dichroism amplitude is consistent with the observations if each disk has 1.25 turns of DNA, and both C_2 axes are parallel to the field (see Figure 9).

Other models for the spacerless dimer are possible. For example, the data agree with a model in which one disk has 1.5 turns of DNA and the other has 1.0 turn. Imagine the two disks in contact through their edges with the two C_2 axes perpendicular to the common diameter shared by the two disks. The reduced dichroism amplitude could result from twisting one disk C_2 axis relative to the other by 60°. In this case each disk could not line up edge-on to the field, but instead would form an angle γ_1 (the cylindrical axis relative to the field) of 60°, yielding a predicted dichroism in agreement with experiment. Further experiments will be required to distinguish among the possibilities.

References

Allen, F. S., & Van Holde, K. E. (1971) *Biopolymers 10,* 865–881.

Blobel, G., & Potter, V. R. (1966) *Science 154,* 1662–1665.

Broersma, S. (1960) *J. Chem. Phys. 32,* 1626–1631.

Ding, D., Rill, R., & Van Holde, K. E. (1972) *Biopolymers 11,* 2109–2124.

Finch, J. T., Lutter, L. C., Rhodes, D., Brown, R. S., Rushton, B., Levitt, M., & Klug, A. (1977) *Nature (London) 269,* 29–36.

Fredericq, E., & Houssier, C. (1973) *Electric Dichroism and Electric Birefringence,* Clarendon Press, Oxford.

Hjelm, R. P., Kneale, G. G., Suau, P., Baldwin, J. P., Bradbury, E. M., & Ibel, K. (1977) *Cell 10,* 139–151.

Hogan, M., Dattagupta, N., & Crothers, D. M. (1978) *Proc. Natl. Acad. Sci. U.S.A. 75,* 195–199.

Klevan, L., & Crothers, D. M. (1977) *Nucleic Acids Res. 4,* 4077–4089.

Klevan, L., Hogan, M., Dattagupta, N., & Crothers D. M. (1977) *Cold Spring Harbor Symp. Quant. Biol. 42,* 207-214.
Klevan, L., Dattagupta, N., Hogan, M., & Crothers, D. M. (1978) *Biochemistry 17* (following paper in this issue).
Koenig, S. H. (1975) *Biopolymers 14,* 2421-2423.
Langmore, J. P., & Wooley, J. C. (1975) *Proc. Natl. Acad. Sci. U.S.A. 72,* 2691-2695.
Levitt, M. (1978) *Proc. Natl. Acad. Sci. U.S.A. 75,* 640-644.
Maestre, M. F., & Kilkson, R. (1965) *Biophys. J. 5,* 275-287.
Minakata, A., Imai, N., & Oosawa, F. (1972) *Biopolymers 11,* 347-359.
O'Konski, C. T., Yoshioka, K., & Orttung, W. H. (1959) *J. Phys. Chem. 63,* 1558-1565.
Pardon, J. F., Worcester, D. L., Wooley, J. C., Tatchell, K., Van Holde K. E., & Richards, B. M. (1975) *Nucleic Acids Res. 2,* 2163-2176.
Rill, R. (1972) *Biopolymers 11,* 1929-1941.
Suau, P., Kneale, G. C., Braddock, G. W., Baldwin, J. P., & Bradbury, E. M. (1977) *Nucleic Acids Res. 4,* 3769-3786.
Tinoco, I. (1955) *J. Am. Chem. Soc. 77,* 4486-4489.

Physical Studies of Nucleosome Assembly†

L. Klevan, N. Dattagupta, M. Hogan, and D. M. Crothers*

ABSTRACT: Biochemical, spectroscopic, and hydrodynamic studies were performed on the reconstituted complex of 140 base pair DNA and the arginine-rich histone tetramer $(H3/H4)_2$. The histones bind to DNA in a 1:1 molar ratio to form a stable particle which orients in an electric field with a rotational correlation time of 6.3 μs and a limiting reduced dichroism of −0.74. The complex was modeled hydrodynamically as a cylinder of dimensions 450 × 80 × 80 Å containing approximately 1.5 superhelical turns. Addition of the lysine-rich histones to this complex causes a condensation of the structure and results in physical properties nearly identical with those of a native nucleosomal particle.

The arginine-rich histones H3 and H4 play a central role in packaging the DNA of eucaryotic chromosomes into an array of repeating subunits or nucleosomes (Oudet et al., 1975). Each nucleosome consists of a central core particle comprising 140 base pairs of DNA and two each of histones H2A, H2B, H3, and H4 (Kornberg, 1974; Olins et al., 1976) along with a spacer region of variable length (Spadafora et al., 1976; Lohr et al., 1977). Comparative studies of histone H4 from pea seedling and calf thymus have demonstrated a remarkable conservation of amino acid sequence for proteins derived from such diverse organisms, suggesting a strong structural-functional correlation for its interaction with DNA (DeLange et al., 1969). Likewise, histone H3 is unique in that it contains the amino acid cystine and may be involved in stabilizing the nucleosome during periods of genetic inactivity (DeLange & Smith, 1972; Camerini-Otero & Felsenfeld, 1977a).

Kornberg & Thomas (1974) reported the isolation of a stable arginine-rich histone tetramer which, when reconstituted with DNA and the lysine-rich histones reproduced the X-ray diffraction pattern of chromatin (Kornberg & Thomas, 1974). The stability of this protein complex was subsequently confirmed by equilibrium centrifugation (Roark et al., 1974; D'Anna & Isenberg, 1974a) and by studies on the reassociation of purified histone components (D'Anna & Isenberg, 1974b).

Physical studies on the histone tetramer indicate a highly asymmetric protein structure; the sedimentation coefficient $s_{20,w}$ is 2.81 and the ratio of the frictional coefficient to that of a sphere of the same volume (f/f_0) is approximately 1.6 (Roarck et al., 1976). Although the molecule contains a considerable amount of α helix, the proton NMR spectrum resembles that of a partially denatured protein (Moss et al., 1976). It has been suggested that the N-terminal cationic regions of these proteins are highly mobile (Lilley et al., 1976) and may be the primary sites of interaction with DNA (Sung & Dixon, 1970; Weintraub et al., 1976). The combination of a globular hydrophobic core and extended N-terminal hydrophilic regions could account for the observed hydrodynamic properties of the molecule (Roark et al., 1976).

Recently it has been demonstrated that the arginine-rich histones can supercoil DNA in the absence of the other histone components. Bina-Stein & Simpson (1977) observed that reconstitution of the histone tetramer with closed circular SV 40 DNA, followed by treatment with relaxing enzyme, could reproduce the superhelical density of virion DNA upon removal of the protein. The results of their study were consistent with the generation of approximately one negative superhelical turn per bound tetramer. Camerini-Otero & Felsenfeld (1977b) observed a significant amount of supercoiling upon reconstituting the tetramer with relaxed Col E1 DNA at a 0.5 g/g of protein/DNA ratio, although a nucleosome equivalent of protein was required to obtain a superhelical density identical with that of native DNA. No supercoiling was observed in either study upon reconstitution of the lysine-rich histones with DNA.

Moss et al. (1977) have obtained X-ray diffraction patterns very similar to that of chromatin from fibers of DNA reconstituted with the arginine-rich histones in a 1:1 weight ratio. It was suggested that these diffraction patterns might result from a structure in which one histone tetramer was bound to approximately 65 base pairs of DNA.

In this paper we report the stoichiometry and hydrodynamic properties of a reconstituted particle of the arginine-rich histones and 140 base pair DNA. In summary of our results, we

† From the Department of Chemistry, Yale University, New Haven, Connecticut 06520. *Received April 21, 1978.* This research was supported by Grant CA15583 from the National Cancer Institute.

0006-2960/78/0417-4533$01.00/0